Available online at www.sciencedirect.com

SciVerse ScienceDirect

Ceramics International 39 (2013) 7029–7035

CERAMICS INTERNATIONAL

www.elsevier.com/locate/ceramint

Carbon nanofibers decorated with binary semiconductor (TiO_2/ZnO) nanocomposites for the effective removal of organic pollutants and the enhancement of antibacterial activities

Bishweshwar Pant[a], Hem Raj Pant[a,b,**], Nasser A.M. Barakat[c], Mira Park[c], Kyungsoo Jeon[c], Yuri Choi[c], Hak-Yong Kim[c,*]

[a]Department of Bionano System Engineering, Chonbuk National University, Republic of Korea
[b]Department of Engineering Science and Humanities, Pulchowk Campus, Tribhuvan University, Nepal
[c]Department of Organic Materials and Fiber Engineering, Chonbuk National University, Republic of Korea

Received 26 December 2012; received in revised form 14 February 2013; accepted 14 February 2013
Available online 27 February 2013

Abstract

A novel photocatalytic and antibacterial carbon nanofiber decorated with TiO_2/ZnO composite NPs was prepared by a simple electrospinning method followed by calcination and hydrothermal treatment. The loading of a small amount of ZnO NPs throughout the fibers prior to electrospinning could provide nucleation sites for the crystal growth of ZnO from its precursor during hydrothermal synthesis and could effectively hold TiO_2/ZnO particles on the surface of the fibers for better stability. The morphology and structure of the as-synthesized particles were characterized by field emission scanning electron microscopy (FE-SEM), transmission electron microscopy (TEM), X-ray diffraction (XRD), and Raman spectroscopy, which revealed that TiO_2/ZnO NPs were attached on the surface of the carbon nanofibers. The as-synthesized nanocomposite exhibited a strong photocatalytic activity for the decomposition of methylene blue (MB) under UV irradiation and showed good antibacterial properties as well. The enhanced photocatalytic performance of the developed nanocomposite can be attributed to the adsorption characteristic of carbon nanofiber and the matched band potentials of TiO_2 and ZnO. The perfect recovery of the catalyst after the reaction and its unchanged efficiency for cyclic use showed that it will be an economical and environmentally friendly photocatalyst.

Keywords: A. Electrospinning; A. Hydrothermal; B. Nanocomposite; E. Photocatalyst; E. Antibacterial

1. Introduction

The use of nanotechnology for the prevention of toxic chemical and microbial contamination may provide solutions for the challenges faced by the health care system in 21st century. Therefore, the development of effective material having both photocatalytic and antimicrobial properties is of great significance. The excessive use of various dyes in the textile industry has led to severe surface water and groundwater contamination from the release of toxic and colored effluents [1]. Semiconductor photocatalysis is one of the advanced physicochemical processes applicable in the photodegradation of environmental organic pollutants and toxics. For the removal of dye pollutants, semiconductor metal oxides, such as TiO_2, ZnO, ZnS, CdS, and Fe_2O_3 nanoparticles (NPs), have thus far been shown to be the most promising materials in this field [2,3]. TiO_2 and ZnO semiconductors have quite similar band gaps (ZnO, 3.37 eV and TiO_2, 3.2 eV) and have become the most extensively used photocatalysts in recent years. They are known as inexpensive, nontoxic, and very effective semiconductor photocatalysts. These photocatalysts are applicable to a wide range of organic synthetic dyes [4]. However, the photo-induced charge carrier in single bare semiconductor

*Corresponding author. Tel.: +82 63 270 2351; fax: +82 63 270 4249.
**Corresponding author. Department of Bionano System Engineering, Chonbuk National University, Republic of Korea.
E-mail addresses: hempant@jbnu.ac.kr (H.R. Pant), khy@jbnu.ac.kr (H.-Y. Kim).

0272-8842/$ - see front matter © 2013 Elsevier Ltd and Techna Group S.r.l. All rights reserved.
http://dx.doi.org/10.1016/j.ceramint.2013.02.041

particles has a very short lifetime because of the high-recombination rate of the photogenerated electron/hole pairs, which reduces photocatalytic efficiency and hinders further use of particles. Therefore, improving photocatalytic activity by modification has become an important task among researchers in recent years. Doping novel metal into the photocatalyst lattice [5,6] and coupling semiconductors [7–9] are effective ways to decrease the e–h recombination process.

In the past decade, a number of studies related to the photocatalytic activity of TiO_2 or ZnO coupled with metal oxides, such as SnO_2 [10–12], WO_3 [10,13], Fe_2O_3 [14], and some rare earth oxides [15], for the purpose of improving the photocatalytic activity of TiO_2 or ZnO. Our previous results also showed that the photocatalytic activity of ZnO/TiO_2 was higher than that of the either material alone [16]. Secondary pollution is one of the problems limiting the widespread applications of the nanostructured photocatalysts [17]. In other words, most of the reported nanostructured photocatalysts can effectively eliminate the organic pollutants; however, they create a serious issue due to the difficulty of separating the utilized nanostructured photocatalysts from the treated water, especially in the case of large-scale processes [18]. In this regard, Chang studied the growth of ZnO nanorods on PI nanofibers via the immobilization of ZnO seeds on PI nanofibers, followed by hydrothermal processing [19]. The post electrospinning loading of ZnO sheets on fibers for nucleation showed poor stability. Therefore, here, ZnO NPs are incorporated into fibers prior to electrospinning for nucleation to achieve better stability.

Carbon nanostructures such as carbon nanofibers (CNFs) and nanotubes (CNTs) have attracted great interest due to their unique anisotropic properties and wide range of potential applications [20]. Besides the known adsorption capacity of the carbonaceous materials, some results have demonstrated that CNFs could efficiently capture and transport photogenerated electrons through highly conductive long CNFs [21,22]. The combined roles of the activated carbon and ZnO/TiO_2 nanocomposite showed a synergistic effect on the efficient degradation of some organic compounds, which is closely related to the enhancement of pollutant adsorption from water because of its extremely high surface area and high microporous volume. Recently, antibacterial activities associated with ZnO nanomaterials have been investigated [23,24]. It has also been reported that ZnO nanoparticles significantly inhibited bacterial growth under normal laboratory light conditions, including even dark conditions. Based on these studies, the synthesized TiO_2/ZnO nanocomposites are expected to exhibit superior antibacterial activity without light irradiation. Moreover, under UV light irradiation, a TiO_2/ZnO composite can provide enhanced antibacterial activity compared with pristine TiO_2 because of the increased recombination time of photogenerated electron–hole pairs [25,26].

Therefore, to exploit the effect of the carbon nanofiber as an adsorbent and the incorporation of TiO_2/ZnO NPs as semiconductor photocatalytic materials and antibacterial agents, here, we have successfully reported the fabrication of ZnO nanoflowers incorporated with carbon nanofibers, which are further loaded with TiO_2 NPs by combined electrospinning and hydrothermal processing. In this study, optimization of the treatment based on TiO_2, ZnO, and carbon nanofibers to achieve the best simultaneous antibacterial efficiency and photodegradation has been targeted.

2. Experimental procedure

2.1. Materials

TiO_2 NPs (Aeroxide P25, 80% anatase 20% rutile, average particle size of 21 nm and specific surface area of $50 \pm 15\ m^2\ g^{-1}$), zinc powder, bis-hexamethylene triamine, zinc nitrate hexahydrate, acetic acid (99.7 assay), N, N-dimethylformamide (DMF, 99.5 assay), and methylene blue were obtained from Showa Co. Japan. Polyacrylonitrile (PAN) with a molecular weight of 150,000 was obtained from Sigma-Aldrich, and ethanol (94.5 assay) was obtained from Samchun Co., South Korea.

2.2. Preparation of carbon nanofibers

The preparation of carbon nanofibers consisted of two steps. First, 10% PAN solution containing 0.1 g of zinc powder was prepared by dissolving the zinc into N, N-dimethylformamide (DMF). After stirring at room temperature for 12 h, the solution was electrospun at 15 kV by maintaining a tip-to-collector distance of 15 cm. As-spun PAN nanofiber were collected in aluminum foil and; vacuum dried at 70 °C for 12 h. For carbonization, the nanofiber were stabilized in air at 250 °C for 3 h and then carbonized under argon at 900 °C for 5 h.

2.3. Incorporation of ZnO–TiO_2 NPs on carbon nanofiber

According to our previous study [16], ZnO nanoflowers containing TiO_2 NPs could be obtained by a hydrothermal treatment of TiO_2 NPs, bis-hexamethylene triamine, and zinc nitrate hexahydrate. Therefore, ZnO nanoflowers with TiO_2 NPs have been grown around the carbon nanofibers using the same strategy. The process was carried out in a stainless steel autoclave with a height of 15 cm and a diameter of 7 cm. Here, 0.5 g of bis-hexamethylene triamine was dissolved in 50 g of water. In another bottle, 0.75 g of zinc nitrate hexahydrate and 20 mg of TiO_2 NPs were dissolved in 50 g of water. These solutions were mixed and 25 mg of carbon nanofibers was added to the mixture. After vigorously stirring for 6 h, the mixture was placed in a Teflon crucible and kept inside the autoclave. The sealed autoclave was maintained at 140 °C for 2 h. The product obtained after cooling was filtered off, washed several times with distilled water and ethanol, and dried at 60 °C for 12 h before analysis.

2.4. Characterization

The surface morphology of nanofibers was studied by using a JEOL JSM-5900 scanning electron microscope; (JEOL Ltd, Japan), and a field-emission scanning electron microscope equipped with EDX (FE-SEM, Hitachi S-7400, Japan). The phase and crystallinity were characterized by using a Rigaku X-ray diffractometer (Rigaku Co., Japan) with Cu Kα ($\lambda = 1.54056$ Å) radiation over a 2θ range of angles, from 10° to 80°. High-resolution images and selected area electron diffraction patterns were observed by a JEOL JEM 2010 transmission electron microscope (TEM) operating at 200 kV(JEOL Ltd, Japan). Raman spectra were obtained using FT-Raman spectroscopy (RFS-100S, Bruker, Germany). The concentration of the dyes during the photodegradation study was investigated by spectroscopic analysis using an HP 8453 UV–visible spectroscopy system (Germany). The spectra obtained were analyzed by the HP ChemiStation 5890 Series software.

2.5. Photocatalytic activity measurements

The photocatalytic activity of the prepared composite nanofiber photocatalysts was evaluated by the degradation of methylene blue aqueous solution under UV-irradiation. The process was carried out in a Petri dish that was equipped with an ultraviolet lamp ($l = 365$ nm). The distance between the Petri dish and the UV lamp was 5 cm. In each case, 25 ml of dye solution (10 ppm concentration) and 20 mg of catalyst were mixed to obtain good dispersion by stirring. After 15 min of stirring, the dye degradation test was carried out without stirring. At specific time intervals, 1 ml of the sample was withdrawn from the system and centrifuged to separate the residual catalyst, and then the absorbance intensity was measured at the corresponding wavelength. For cycling use experiments, the sample were separated from the suspended solution by repeated centrifuging and washing. The mixture underwent three consecutive cycles. After each cycle, the catalyst was filtered and washed thoroughly with water, and fresh MB solution of the same concentration was used.

2.6. Antibacterial properties

Antibacterial testing was carried out using an *Escherichia coli* (*E. coli*) suspension under UV radiation with an intensity of 10%. The working suspensions were prepared by adding 200 µl of inoculated LB medium to 50 ml of sterilized, distilled water in a beaker. The antibacterial experiment was carried out in a sterilized 100 ml glass beaker containing *E. coli* suspension (50 ml) and 0.4 g/l of different photocatalysts with magnetic stirring. The initial bacterial concentration was maintained at 107 CFU/ml, and the tests were performed at room temperature for 120 min. At given time intervals, 1 ml of the suspension was collected and diluted appropriately by serial dilution in distilled water. To count the bacterial concentration, ready-to-use petrifilm (3 M Petrifilm, USA) and prepared agar plates were used. After incubation for 48 h, the number of bacteria was manually counted using a colony counter. Furthermore, the antibacterial activity of as-synthesized particles without UV light was measured by applying the zone inhibition method to *E. coli*. Using a spread plate method, nutrient agar plates were incubated with 1 ml of bacterial suspension containing approximately 106 colony-forming units (CFU)/ml. The photocatalysts were gently placed on the inoculated plates, and were then incubated at 37 °C for 24 h. Zones of inhibition were determined by measuring the clear area formed around each photocatalyst.

3. Results and discussion

Fig. 1 shows FE-SEM micrographs of a PAN nanofiber and its carbonized product. PAN precursor nanofibers exhibit smooth surface morphology with a uniform diameter approximately 470 nm (Fig. 1A). After stabilization and carbonization, the diameter of nanofiber decreases to 280 ± 10 nm. The reduction in the diameter of the nanofibers may be due to degradation of the polymer by heat treatment during the conversion to carbon nanofibers. Fig. 2 represents the morphology of the obtained TiO_2-doped ZnO nano-flower and carbon nanofiber containing TiO_2/ZnO NP respectively. Our previous work [16] showed that the addition of TiO_2 in ZnO decreases its size from the micro to the nano-scale (Fig. 2a and b). Here, the size

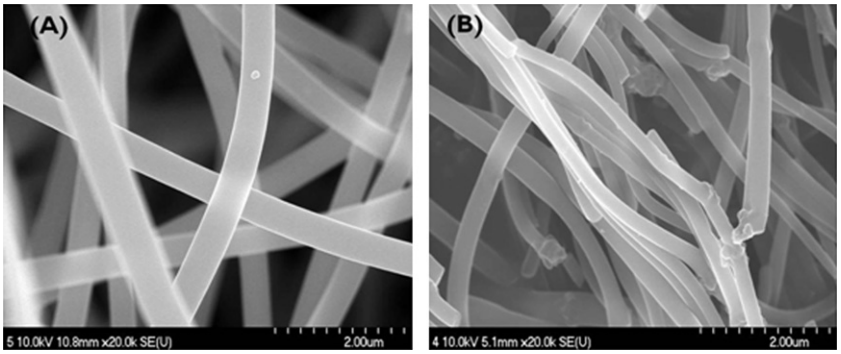

Fig. 1. FE-SEM images of PAN nanofibers (A) and carbon nanofibers (B).

of the nanoparticles further decreases from the addition of carbon nanofibers to the same system (Fig. 2c). The presence of carbon nanofibers could hinder the agglomeration of crystallized ZnO particles during hydrothermal process. Furthermore, addition of carbon fibers into the same volume could decrease the concentration of ZnO precursor per unit volume and consequently decreased the size of ZnO NPs [6]. The nanoparticles were found to attach on the surface of carbon nanofibers with well distribution. The formation of ZnO particles and their growth might be hindered when TiO_2 NPs and carbon nanofibers are present in hydrothermal treatment. Furthermore, the TEM image in Fig. 2d confirms that the anchored TiO_2/ZnO nanoflowers were obviously sintered on carbon nanofibers during the hydrothermal treatment. The particles that formed the nanoflower were very uniform.

Fig. 3A represents typical XRD patterns for the different samples obtained from the electrospinning process, carbonization, and the hydrothermal process. The diffraction peak of the PAN fibers occurs at approximately $2\theta = 17^\circ$, which corresponds to a planar spacing $d = 5.240$ Å and can be indexed to the (100) plane of a hexagonal structure [27]. After the carbonization process, this diffraction peak totally disappears. Meanwhile, a new broad peak appears at approximately $2\theta = 25^\circ$, indicating the formation of a graphite structure [28,29]. In carbon–TiO_2/ZnO, the apparent peaks at 2θ values of 31.8, 34.5, 36.4, 47.6, 56.6, 62.8, 66.3, 68.1, 69, and 76.88 correspond to the crystal planes of (100), (002), (101), (102), (110), (103), (200), (112), (201), and (202), confirming the formation of pure ZnO, which was found to be similar to that reported in our previous work [16]. The presence of sharp peak at $2\theta = 25^\circ$ (crystal plane 101, for the rutile phase of TiO_2) in the nanocompo-

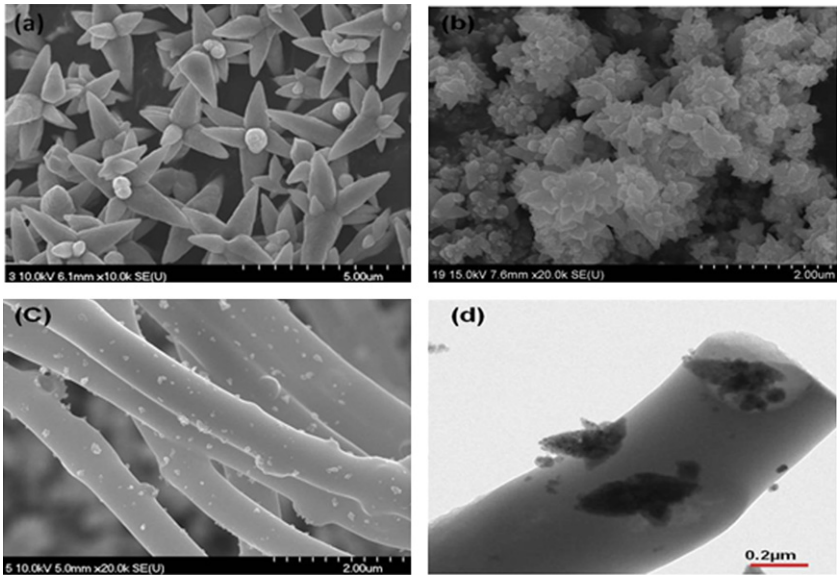

Fig. 2. FE-SEM images of pristine ZnO microflowers (a); ZnO flowers containing TiO_2 NPs (b), and FE-SEM and TEM images of carbon–TiO_2/ZnO nanocomposites (c and d, respectively).

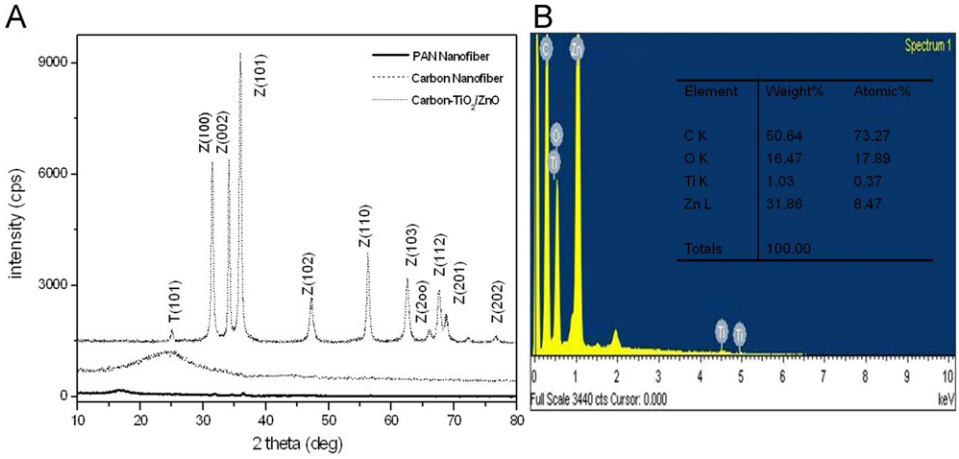

Fig. 3. XRD spectra (A) and FESEM–EDS (B).

site revealed that TiO_2 is well-doped on the surface of the ZnO nanoflowers with carbon as a base. Furthermore, EDX results obtained from FE-SEM images (Fig. 3b) confirm the incorporation of TiO_2/ZnO nanoflowers in carbon nanofibers and simultaneously supports the XRD analysis. Raman spectroscopy was used to analyze the chemistry of the obtained carbon. As shown in Fig. 4, there were two broad peaks centered at approximately 1350 and 1590 cm^{-1}. These two peaks correspond to the well-known D and G bands of graphite, respectively [30–32], indicating that the PAN nanofiber was transformed into graphite with a fraction of disordered sp^2 C–C bonding. Aside from these peaks, the extra peaks at approximately 339 and 639 cm^{-1} confirm the presence of TiO_2 [33,34], and the peaks at 331, 381, 437, and 577 represent ZnO [35].

To elucidate the effect of coupling TiO_2 with ZnO particles and carbon nanofibers, the photocatalytic activity was measured by using MB dye. Decolorization of the methylene blue dye was carried out under UV irradiation. As shown in Fig. 5A, the rate of degradation of methylene blue is significantly enhanced by the as-prepared carbon–TiO_2/ZnO photocatalyst. The enhanced degradation of methylene blue in this experiment, could be confirmed by comparing the obtained results with our previous work [16] because all the conditions (except carbon nanofibers) were similar in these two works. The higher photocatalytic activity of TiO_2/ZnO nanostructures combined with carbon nanofibers compared with other photocatalysts is attributed mainly to the coupling effect of TiO_2 and ZnO and to the adsorption property of the carbon nanofibers. The photogenerated electrons enter the conduction band of TiO_2 from the conduction band of the excited ZnO. Similarly, the photogenerated hole is also transferred from the valence band of TiO_2 to the valence band of ZnO. Such an efficient charge separation increases the lifetime of the charge carriers and increases the efficiency of the interfacial charge transfer to adsorbed substrates. Therefore, the photocatalytic properties increase because the possibility of recombination between photogenerated electrons and holes is reduced by facilitating their separation [36–38]. Moreover, carbon nanofiber supported catalysts are believed to exhibit cooperative or synergetic effects between CNFs and catalyst systems [39].

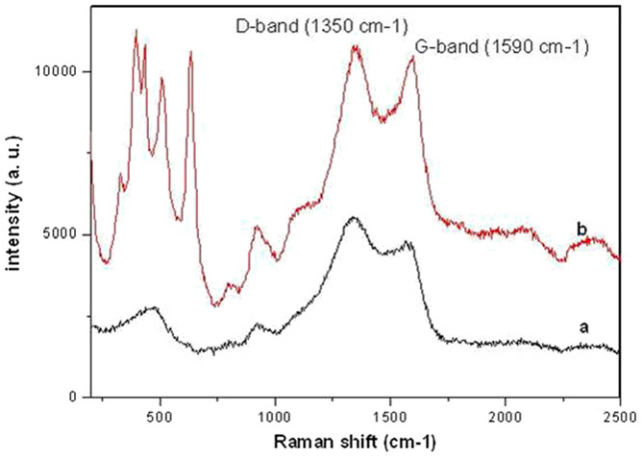

Fig. 4. Raman spectra showing D and G bands of carbon (a) and carbon–TiO_2/ZnO (b).

To verify the reusability of the carbon–TiO_2/ZnO nanocomposite, we carried out three successive cyclic tests with the same nanocomposite. More specifically, the same sample (20 mg) was used to successively treat 25 ml of the dye solution (10 ppm). Fig. 5B shows the cyclic degradation results of MB under UV irradiation. As shown in the figure, the efficacies of the initially used and reused composite photocatalyst were similar for MB degradation for first and second cycle. However, the efficacy was lower in the third cycle. It is known that exhaustion of adsorbates is the main problem facing the widespread utilization of the adsorption technique in water treatment processes. In other words, the organic pollutants block the active sites in the adsorbent materials which may be the cause of reduced degradation of MB in the third cycle.

The effect of the obtained binary semiconductor composite on the antibacterial efficiency was measured using mild UV irradiation of a bacterial solution at room temperature. Fig. 6 shows the antibacterial effect of the as-prepared photocatalyst under mild (10% intensity) UV radiation. The figure shows

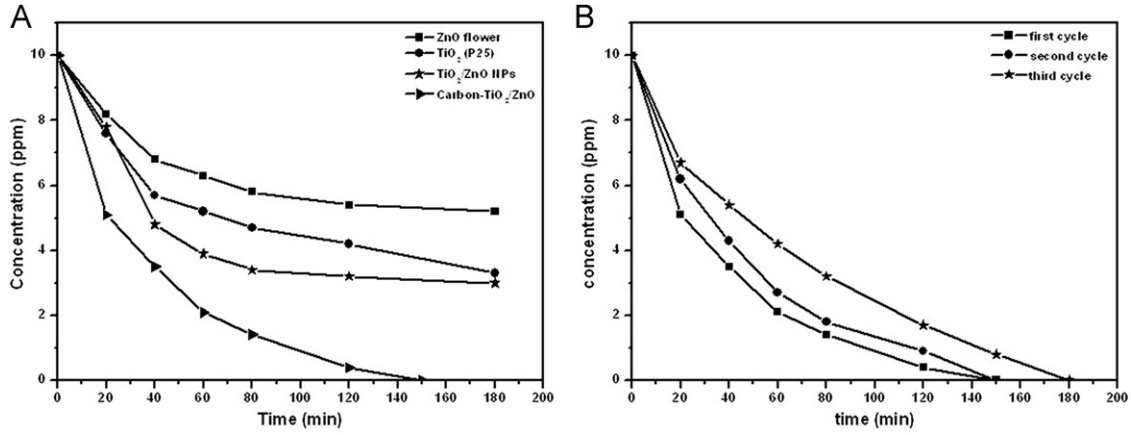

Fig. 5. Comparison of the MB photodegradation in different specimens under UV radiation (A) and the catalytic reusability efficiency of carbon–TiO_2/ZnO nanocomposite up to three cycles (B).

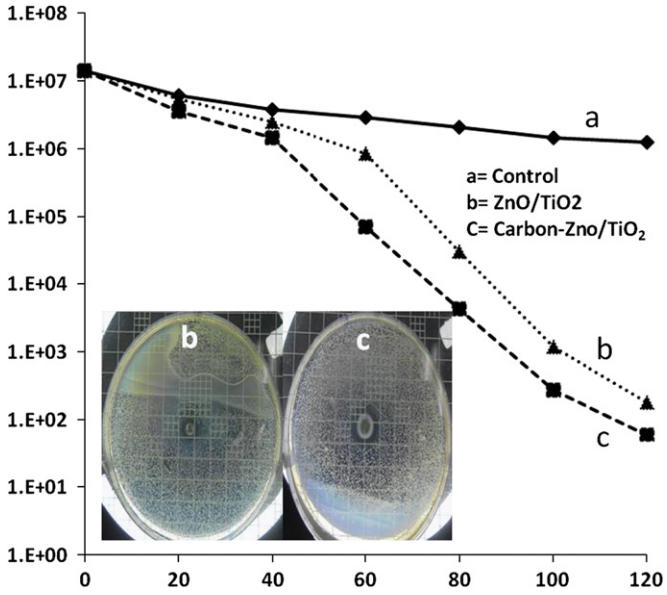

Fig. 6. Antibacterial efficiency of different photocatalysts for gram-negative *E. coli* bacteria under mild UV radiation. Insets are the respective zones of inhibition.

that carbon–TiO_2/ZnO has a stronger antimicrobial effect than that of the TiO_2/ZnO nanocomposite. Notably, the growth of *E. coli* on the control plate decreased after UV irradiance, mostly due to the biocidal effect of the UV light. The TiO_2/ZnO nanocomposite increased the formation of reactive hydroxyl radicals compared with pure TiO_2 and ZnO nanofibers when exposed to UV irradiation due to the enhanced recombination times of the electron–hole pairs [40]. Consequently, the TiO_2/ZnO nanocomposite showed significant antibacterial activity due to increasing numbers of reactive hydroxyl radicals and the bactericidal effect of ZnO itself. These radicals can react with DNA, cell membranes, and cellular proteins, leading to cell death. The larger diameter of the inhibition zone (DIZ) in carbon–TiO_2/ZnO compared with the DIZ of TiO_2/ZnO clearly revealed the role of carbon nanofibers in determining the antibacterial properties of the composite because the size of the TiO_2/ZnO nanoflowers was decreased by the addition of carbon nanofibers during hydrothermal processing. The nanometer scale of the carbon–TiO_2/ZnO nanocomposites could enhance their antibacterial performance due to the large surface area. Based on these data, it can be concluded that carbon–TiO_2/ZnO nanocomposites have effective synergistic antimicrobial properties under UV irradiation.

4. Conclusions

Successful preparation of carbon nanofibers containing distributed TiO_2/ZnO was achieved by the carbonization of electrospun PAN nanofibers and hydrothermal processing. The advantage of this strategy lies in its adsorption ability, fast degradation of dye, and antibacterial performance. The combination of the high surface area of carbon nanofibers and the photocatalytic property of the TiO_2/ZnO system make this composite a promising material for air and water purification.

Acknowledgments

This research was financially supported by the Ministry of Education, Science and Technology (MEST) and National Research Foundation of Korea (NRF) through Leaders in Industry–University Cooperation and the Human Resource Training Project for Regional Innovation. This work was also supported by IT R&D program of MKE/KEIT (10041957, Design and Development of fiber-based flexible display). We thank Ms. Eunjeong Shin and Mr. Jong-Gyun Kang, Center for University Research Facility, for taking high-quality FE-SEM and TEM images respectively.

References

[1] I.A. Salem, M.S. El-Maazawi, Kinetics and mechanism of color removal of methylene blue with hydrogen peroxide catalyzed by some supported alumina surfaces, Chemosphere 41 (2000) 1173–1180.
[2] I. Poulios, E. Micropoulou, R. Panou, E. Kostopoulou, Photooxidation of eosin Y in the presence of semiconducting oxide, Applied Catalysis B 41 (2003) 345–355.
[3] C. Lizama, J. Freer, J. Baeza, H.D. Mansilla, Optimized photodegradation of Reactive Blue 19 on TiO_2 and ZnO suspensions, Catalysis Today 76 (2002) 235–246.
[4] M.M. Uddin, M.A. Hasnat, A.J.F. Samed, R.K. Majumdar, Influence of TiO_2 and ZnO photocatalysts on adsorption and degradation behaviour of Erythrosine, Dyes and Pigments 75 (2007) 207–212.
[5] H.M. Coleman, K. Chiang, R. Amal, Effects of Ag and Pt on photocatalytic degradation of endocrine disrupting chemicals in water, Chemical Engineering Journal 113 (2005) 65–72.
[6] H.R. Pant, B. Pant, R.K. Sharma, A. Amarjargal, H.J. Kim, C.H. Park, L.D. Tijing, C.S. Kim, Antibacterial and photocatalytic properties of Ag/TiO_2/ZnO nano-flowers prepared by facile one-pot hydrothermal process, Ceramics International 39 (2013) 1503–1510.
[7] S. Sakthivel, B. Neppolian, M.V. Shankar, B. Arabindoo, Solar photocatalytic degradation of azo dye: comparison of photocatalytic efficiency of ZnO and TiO_2, Solar Energy Materials and Solar Cells 77 (2003) 65–82.
[8] C.H. Wu, Comparison of azo dye degradation efficiency using UV/single semiconductor and UV/coupled semiconductor systems, Chemosphere 57 (2004) 601–608.
[9] D.L. Liao, C.A. Badour, B.Q. Liao, Preparation of nanosized TiO_2/ZnO composite catalyst and its photocatalytic activity for degradation of methyl orange, Journal of Photochemistry and Photobiology 194 (2008) 11–19.
[10] S.F. Chen, L. Chen, The preparation of coupled SnO_2/TiO_2 photocatalyst by ball milling, Materials Chemistry and Physics 98 (2006) 116–120.
[11] K.V. Gopal, P.V. Kamat, Enhanced rates of photocatalytic degradation of an azo dye using SnO_2/TiO_2 coupled semiconductor thin films, Environmental Science & Technology 29 (1995) 841–845.
[12] K. Tennakone, J. Bandara, Photocatalytic activity of dye-sensitized tin(IV) oxide nanocrystalline particles attached to zinc oxide particles: long distance electron transfer via ballistic transport of electrons across nanocrystallites, Applied Catalysis A: General 208 (2001) 335–341.
[13] X.Z. Li, F.B. Li, C.L. Yang, W.K. Ge, Photocatalytic activity of WO*x*–TiO_2 under visible light irradiation, Journal of Photochemistry and Photobiology A: Chemistry 141 (2001) 209–217.

[14] B. Pal, M. Sharon, G. Nogami, Preparation and characterization of TiO_2/Fe_2O_3 binary mixed oxides and its photocatalytic properties, Materials Chemistry and Physics 59 (1999) 254–261.
[15] J. Lin, J.C. Yu, An investigation on photocatalytic activities of mixed TiO_2-rare earth oxides for the oxidation of acetone in air, Journal of Photochemistry and Photobiology A: Chemistry 116 (1998) 63–67.
[16] H.R. Pant, C.H. Park, B. Pant, L.D. Tijing, H.Y. Kim, C.S. Kim, Synthesis, characterization, and photocatalytic properties of ZnO nano-flower containing TiO_2 NPs, Ceramics International 38 (2012) 2943–2950.
[17] H.R. Pant, D.R. Pandeya, K.T. Nam, W.I. Baek, S.T. Hong, H.Y. Kim, Photocatalytic and antibacterial properties of a TiO_2/nylon-6 electrospun nanocomposite mat containing silver nanoparticles, Journal of Hazardous Materials 189 (1–2) (2011) 465–471.
[18] H.R. Pant, B. Pant, P. Pokharel, H.J. Kim, L.D. Tijing, C.H. Park, D.S. Lee, H.Y. Kim, C.S. Kim, Photocatalytic TiO_2-RGO/nylon-6 spider-wave-like nano-nets via electrospinning and hydrothermal treatment, Journal of Membrane Science 429 (2013) 225–234.
[19] Z. Chang, Firecracker-shaped ZnO/polyimide hybrid nanofibers via electrospinning and hydrothermal process, Chemical Communications 47 (2011) 4427–4429.
[20] F.L. Darkrim, P. Malbrunot, G.P. Tartaglia, Review of hydrogen storage by adsorption in carbon nanotube, International Journal of Hydrogen Energy 27 (2002) 193–202.
[21] H.E. Unalan, D. Wei, K. Suzuki, S. Dalal, P. Hiralal, H. Matsumoto, S. Imaizumi, M. Minagawa, A. Tanioka, A.J. Flewitt, W.I. Milne, G.A.J. Amaratunga, Photoelectrochemical cell using dye sensitized zinc oxide nanowires grown on carbon fibers, Applied Physics Letters 93 (2008) 133116.
[22] J. Liu, J. Li, A. Sedhain, J. Lin, H. Jiang, Structure and photoluminescence study of TiO_2 nanoneedle texture along vertically aligned carbon nanofiber arrays, Journal of Physical Chemistry C 112 (2008) 17127–17132.
[23] O. Yamamoto, Influence of particle size on the antibacterial activity of zinc oxide, International Journal of Inorganic Materials 3 (2001) 643–646.
[24] Q.L. Li, S. Mahendra, D.Y. Lyon, L. Brunet, M.V. Liga, D. Li, P.J.J. Alvarez, Antimicrobial nanomaterials for water disinfection and microbial control: potential applications and implications, Water Research 42 (2008) 4591–4602.
[25] H.R. Pant, C.H. Park, P. Pokharel, L.D. Tijing, D.S. Lee, C.S. Kim, ZnO micro-flowers assembled on reduced grapheme sheets with high photocatalytic activity for removal of pollutants, Powder Technology 235 (2013) 853–858.
[26] S.H. Hwang, J. Song, Y. Jung, O.Y. Kweon, H. Song, J. Jang, Electrospun ZnO/TiO_2 composite nanofibers as a bactericidal agent, Chemical Communications 47 (2011) 9164–9166.
[27] T.H. Ko, C.H. Lin, H.Y. Ting, Structural changes and molecular motion of polyacrylonitrile fibers during pyrolysis, Journal of Applied Polymer Science 37 (1989) 553–566.
[28] A.K. Gupta, D.K. Paliwal, P. Bajaj, Acrylic precursors for carbon fibers, Journal of Macromolecular Science–Reviews in Macromolecular Chemistry & Physics 31 (1991) 1–89.
[29] J. Mu, C. Shao, Z. Guo, Z. Zhang, M. Zhang, P. Zhang, B. Chen, Y. Liu, High photocatalytic activity of ZnO-carbon nanofiber heteroarchitectures, Applied Materials & Interfaces 3 (2011) 590–596.
[30] Y. Wang, S. Serrano, J.J. Santiago-Aviles, Conductivity measurement of electrospun PAN based carbon nanofiber, Journal of Materials Science 21 (2002) 1055–1057.
[31] E. Zussman, X. Chen, W. Ding, L. Calabri, D.A. Dikin, J.P. Quintana, R.S. Ruoff, Mechanical and structural characterization of electrospun PAN-derived carbon nanofibers, Carbon 43 (2005) 2175–2185.
[32] C.S. Sharma, R. Vasita, D.K. Upadhyay, A. Sharma, D.S. Katti, R. Venkataraghavan, Photoresist derived electrospun carbon nanofibers with tunable morphology and surface properties, Industrial & Engineering Chemistry Research 49 (2010) 2731–2739.
[33] H.C. Choi, Y.M. Jung, S.B. Kim, Characterization of Raman spectra of size-selected TiO_2 nanoparticles by two-dimensional correlation spectroscopy, Bulletin of the Korean Chemical Society 25 (2004) 426–428.
[34] H.C. Choi, Y.M. Jung, S.B. Kim, Size effects in the Raman spectra of TiO_2 nanoparticles, Vibrational Spectroscopy 37 (2005) 33–38.
[35] M. Rajalakshmi, A.K. Arora, B.S. Bendre, S. Mahamuni, Journal of Applied Physics 87 (2000) 2445–2448.
[36] D.L. Liao, C.A. Badour, B.Q. Liao, Journal of Photochemistry and Photobiology A 11 (2008) 194.
[37] C.W. Zou, X.D. Yan, J. Han, R.Q. Chen, J.M. Bian, E. Haemmerle, W. Gao, Preparation and enhanced photoluminescence property of ordered ZnO/TiO_2 bottlebrush nanostructures, Chemical Physics Letters 476 (2009) 84–88.
[38] M.W. Xiao, L.S. Wang, Y.D. Wu, X.J. Huang, Z. Dang, Nanotechnology 19 (2008) 015706.
[39] K. Rajeshwar, M.E. Osugi, W. Chanmanee, C.R. Chenthamarakshan, M.V.B. Zanoni, P. Kajitvichyanukul, R. Krishnan-Ayer, Heterogeneous photocatalytic treatment of organic dyes in air and aqueous media, Journal of Photochemistry and Photobiology C: Photochemistry Reviews 9 (2008) 171–192.
[40] R. Liua, H. Yea, X. Xiong, H. Liua, Materials Chemistry and Physics 121 (2010) 432–439.